Assessment of the Fibrotic Myocardial Tissue Mechanics by Image Processing

Lucilio Cordero-Grande[1], Teresa Sevilla[2], Ana Revilla[2],
Marcos Martín-Fernández[1], C Alberola-López[1]

[1] Laboratorio de Procesado de Imagen, Universidad de Valladolid, Spain
[2] Instituto de Ciencias del Corazón, Hospital Clínico Universitario de Valladolid, Spain

Abstract

We propose an image processing methodology to study the mechanical properties of fibrotic and normal tissue of the myocardium in magnetic resonance. The procedure fuses cine and late enhanced images and estimates the myocardial motion in cine images. A novel fast and robust tracking procedure is proposed in which the deformation is modeled by a Markov random field and quasi-incompressible, spatio-temporally smooth and homeomorphic transformations are promoted. The method has been applied to the analysis of the differences in the contractility patterns of hyperenhanced and normal zones in a set of 12 *patients affected by hypertrophic cardiomyopathy. The absolute value of both the mean radial and circumferential components of the peak Green strain and strain rate tensors has been encountered significantly lower when hyperenhancement is present. On the other hand, the peak rotation dispersion in the longitudinal-radial plane has been encountered significantly smaller in the fibrotic region.*

1. Introduction

The relationship between myocardial fibrosis and local mechanics is important for the diagnosis and treatment of cardiomyopathies [1]. Imaging techniques provide essential information for the study of these factors and, from them, cardiac magnetic resonance (MR) is increasingly becoming the standard technique as it enables to assess the myocardial morphology, function and structure. Its use is especially relevant for quantitative analysis, as it overcomes the major limitations of echocardiography. From the set of MR acquisition techniques, cine MR and, more specifically, MR tagging and others, let myocardial material points be tracked through the cardiac cycle, therefore enabling to characterize the cardiac dynamics. On the other hand, late-enhanced (LE) MR is able to image the extent of fibrotic tissue in the myocardium, thus revealing its structural impairment.

In this paper, as an exemplary application, we are interested in characterizing the myocardial deformation of fibrotic or hyperenhanced regions in hypertrophic cardiomyopathy (HCM). Hyperenhancement in HCM usually appears at the zone of maximum hypertrophy and at the level of the midventricular septum, specifically in the insertion zones of the right ventricle into the septum. The mechanisms by which this pattern of hyperenhancement appears are currently unknown. Namely, in a study made on 333 HCM patients, Maron et al. found a relationship between the presence of LE and the hypertrophy level, but the LE volume percentage was not associated either with the maximum wall thickness or with the number of hypertrophied segments, so that they concluded that the pathogenesis of these LE areas is not fully resolved [2]. Imaging studies on the relationship between myocardial mechanics and presence of fibrosis in HCM are limited. Some of them, such as [3], have compared a global measure of fibrosis (in this case interstitial fibrosis as given by T_1-mapped images) and a *global* measure of the myocardial mechanical properties without encountering an association between them. In [4], the global longitudinal strain was found to correlate with the global presence of LE hyperenhancement. Something similar occurs in [5], that evaluates the *regional* longitudinal strain and the presence of hyperenhancement in those regions, founding a relationship between the strain and the amount of replacement fibrosis. Finally, in [6], T_1 values were found correlated with circumferential strain values in patients affected both by HCM and dilated cardiomyopathy.

Our approach is somewhat different in that we perform a *local* analysis, which fuses the information of cine and LE MR to provide more insight into the mechanical properties of the fibrotic tissue in HCM. Thus, we propose a method to perform myocardial material point tracking in cardiac cine MR imaging. This modality is selected instead of motion-sensitive MR modalities because it is generally acquired in a conventional cardiac protocol. Once motion features are extracted for the whole myocardium, their differences in fibrotic and normal tissue are characterized by using the fused information coming from the LE MR acquisition. In §2, we introduce the databases used for validation and perform a high-level description of the

proposed image processing algorithm. In §3 we present the experiments performed for the assessment of the mechanical properties of fibrotic regions. We end with some conclusions in §4.

2. Materials and methods

2.1. Materials

Two samples acquired with a GE Genesis Signa 1.5 T equipment are used for validation. The first sample consists of 7 patients affected either by ischemic, hypertrophic, or non-compacted cardiomyopathy. A short axis (SA) cine Steady State Free Precession dataset of each patient is acquired where the myocardium has been manually segmented at end diastole (ED). Additionally, two long axis (LA) 2D images are acquired to correct for breath motion artifacts. The second sample consists of 12 patients affected by HCM. Both SA and LA images are also acquired in this case and a Gadolinium LE SA MR dataset is used to determine the fibrotic regions. Resolution details on these samples are included in Table 1, 30 temporal phases are acquired in the case of cine images, and no slice gaps are present.

Table 1. Details on the samples of MR images used in the paper. Δ_P: pixel resolution. Δ_T: slice thickness.

		Sample 1	Sample 2
cine SA	Δ_P (mm)	$1.48 - 1.64$	$0.64 - 1.64$
	Δ_T (mm)	10	10
cine LA	Δ_P (mm)	$1.56 - 1.80$	$0.78 - 1.87$
	Δ_T (mm)	8	8
LE	Δ_P (mm)	—	$0.48 - 1.64$
	Δ_T (mm)	—	8

2.2. Methods

The processing pipeline is represented in Figure 1. Its main steps are:

1. **3D interpolation**. We use the method in [7] to obtain a quasi-isotropic reconstruction of the cine SA and LE images according to the principles described in [8]. In addition, the same procedure is applied to the distance transform of a set of manually segmented contours on the SA slices to obtain a 3D mask of the myocardial volume.
2. **Alignment**. Some patients were unable to maintain the apnea during the SA studies. Therefore, for correcting misalignments between slices, two manual segmentations of the myocardium in the LA acquisitions are used as reference and the 3D reconstruction of the myocardial surface is aligned against them by using the transform introduced in [8]. As for the alignment of LE volumes against the aligned SA cine volumes, we used the method in [8] applied to the intensity information.
3. **Marching cubes**. This algorithm is used to convert the 3D mask of the myocardial volume to a high resolution representation of the myocardial surface.
4. **Remeshing**. The method in [9] is applied to obtain a triangulation of the myocardial surface with an adequate resolution to apply the tracking method.
5. **Constrained Delaunay Tetrahedralization** (CDT). A tetrahedralization of the myocardial volume is obtained from the surface triangulation using [10].
6. **Tracking**. The tracking method has been recently proposed in [11]. It makes use of a multiresolution Markov random field of discrete 3D deformations defined on a tetrahedral grid of the myocardial volume. A block-matching procedure is combined with biomechanics-based and spatio-temporal smoothness assumptions on the resulting deformations, which are guaranteed to be homeomorphic. The method was validated both visually and by its comparison with manual segmentations (see §3.1).
7. **Fibrosis segmentation**. By using a semi-automatic segmentation, scar is defined as those voxels of the myocardium whose intensity is above a given threshold. In addition, connected components below a predefined number of voxels are considered false positives.
8. **Mechanical description**. We study different features extracted from the trajectories of the material points obtained after tracking. Suppose that a given material point $\mathbf{X}$ at the reference configuration ($t = 0$), usually at ED, follows the trajectory given by $\mathbf{x}(\mathbf{X}, t)$. The Green strain tensor (ST) is obtained from the deformation gradient tensor $\mathbf{F}(\mathbf{X}, t) = \partial \mathbf{x}(\mathbf{X}, t)/\partial \mathbf{X}$ as $\mathbf{E}(\mathbf{X}, t) = (1/2)(\mathbf{F}(\mathbf{X}, t)^T \mathbf{F}(\mathbf{X}, t) - \mathbf{I})$, with $\mathbf{I}$ the identity matrix. The strain rate tensor is defined as $\mathbf{E}'(\mathbf{X}, t) = \partial \mathbf{E}(\mathbf{X}, t)/\partial t$. If a unitary coordinate system is defined adapted to the geometry of the myocardium at ED, such as a radial-circumferential-longitudinal coordinate system $\{\mathbf{R}, \mathbf{C}, \mathbf{L}\}$, one obtains the contraction of (for instance) the ST along a pair of coordinates (in this case the pair formed by taking $\mathbf{R}$ twice) as $E^{\mathbf{RR}}(\mathbf{X}, t) = \mathbf{R}(\mathbf{X})^T \mathbf{E}(\mathbf{X}, t) \mathbf{R}(\mathbf{X})$. Finally, a local coordinate at ED (for instance $\mathbf{R}$) is transformed through time according to $\mathbf{r}(\mathbf{X}, t) = \mathbf{F}(\mathbf{X}, t)\mathbf{R}(\mathbf{X})$, so that, in the plane $\mathbf{RC}$, the coordinates $\mathbf{r}$ and $\mathbf{c}$ would have experienced a rotation of $\alpha^{\mathbf{RCr}}(\mathbf{X}, t) = \arctan\big(\mathbf{C}(\mathbf{X})^T \mathbf{r}(\mathbf{X}, t)/\mathbf{R}(\mathbf{X})^T \mathbf{r}(\mathbf{X}, t)\big)$, $\alpha^{\mathbf{RCc}}(\mathbf{X}, t) = \arctan\big(-\mathbf{R}(\mathbf{X})^T \mathbf{c}(\mathbf{X}, t)/\mathbf{C}(\mathbf{X})^T \mathbf{c}(\mathbf{X}, t)\big)$.
9. **Statistical analysis**. We denote

$$\overline{F}_m(t) = \frac{\int_\Omega F(\mathbf{X}, t)^m d\mathbf{X}}{\int_\Omega d\mathbf{X}} \tag{1}$$

to the m-power spatial average of a mechanical feature F on Ω. We extract these averages inside (Ω_S) and out-

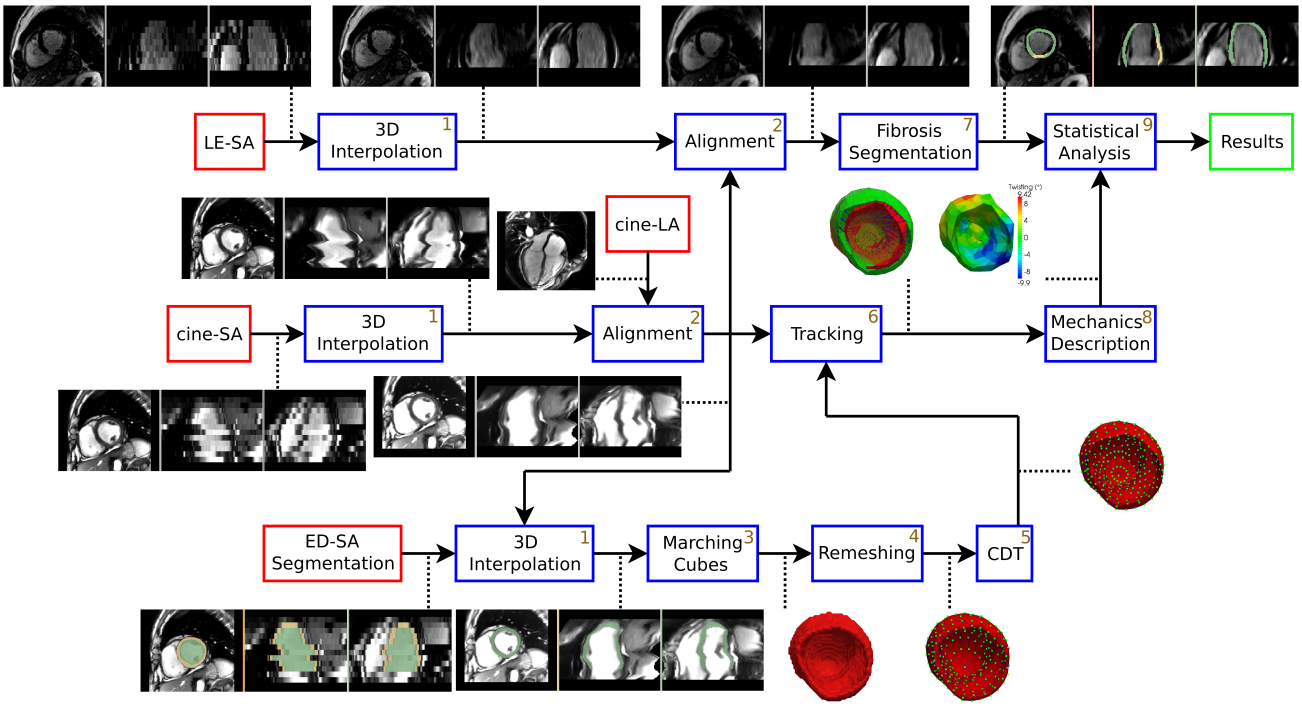

Figure 1. Flowchart of the image processing methodology.

side ($\Omega_{\overline{S}}$) the fibrotic region. For both regions, we introduce the variables $\overline{F}_{m,\max} = \max_t \overline{F}_m(t)$ and $\overline{F}_{m,\min} = \min_t \overline{F}_m(t)$ to characterize the peak behavior of the mechanical features. A Wilcoxon signed-rank test is performed on some of these variables (sampled from Sample 2 on Table 1) to search for significant differences in the mechanical behavior of fibrotic and normal regions.

3. Results

3.1. Validation of the tracking procedure

The ability of the method to track the endocardial, epicardial and myocardial surfaces is evaluated by comparing its results with respect to manual segmentations at end systole in the Sample 1. The 3D Dice coefficient (DC) is used for comparison. Results show a mean±std. DC of 0.858 ± 0.037 for the endocardium, 0.908 ± 0.020 for the epicardium and 0.823 ± 0.041 for the myocardium. In general they seem precise enough, as we have observed that the major inconsistencies are attributable to the incomplete information near the base.

3.2. Mechanics of the fibrotic tissue

The results on the analysis of the mechanics of the fibrotic tissue, by using the Sample 2 and the methodology presented in §2.2, are included in Table 2.

Table 2. Normal ($\Omega_{\overline{S}}$) and fibrotic (Ω_S) tissue mechanics. Statistically significant results ($p < 0.05$) are boldfaced.

Parameter	$\Omega_{\overline{S}}$	Ω_S	p
$\overline{E}^{\mathbf{RR}}_{1,\max}$ (%)	$\mathbf{25.3 \pm 11.7}$	$\mathbf{13.8 \pm 16.5}$	**0.03**
$\overline{E}^{\mathbf{CC}}_{1,\min}$ (%)	$\mathbf{-7.7 \pm 1.4}$	$\mathbf{-5.4 \pm 2.7}$	**0.01**
$\overline{E}^{\mathbf{LL}}_{1,\min}$ (%)	-3.4 ± 4.2	-2.3 ± 5.9	0.52
$\overline{E}'^{\mathbf{RR}}_{1,\max}$ (%/s)	$\mathbf{244 \pm 78}$	$\mathbf{174 \pm 113}$	**0.03**
$\overline{E}'^{\mathbf{CC}}_{1,\min}$ (%/s)	$\mathbf{-113 \pm 12}$	$\mathbf{-96 \pm 27}$	**0.03**
$\overline{E}'^{\mathbf{LL}}_{1,\min}$ (%/s)	-125 ± 16	-113 ± 36	0.18
$\overline{\alpha}^{\mathbf{RCr}}_{2,\max}$ (deg^2)	16.1 ± 6.1	15.6 ± 15.3	0.73
$\overline{\alpha}^{\mathbf{RCc}}_{2,\max}$ (deg^2)	16.3 ± 6.2	15.7 ± 15.2	0.73
$\overline{\alpha}^{\mathbf{CLc}}_{2,\max}$ (deg^2)	2.2 ± 0.8	2.6 ± 1.7	0.38
$\overline{\alpha}^{\mathbf{CLl}}_{2,\max}$ (deg^2)	2.2 ± 0.8	2.7 ± 1.6	0.34
$\overline{\alpha}^{\mathbf{LRl}}_{2,\max}$ (deg^2)	$\mathbf{3.2 \pm 1.5}$	$\mathbf{1.9 \pm 1.7}$	**0.03**
$\overline{\alpha}^{\mathbf{LRr}}_{2,\max}$ (deg^2)	$\mathbf{3.2 \pm 1.6}$	$\mathbf{2.0 \pm 1.8}$	**0.04**

First of all, regarding the maximum strain, we observe that the absolute value of the radial and circumferential components has been encountered significantly smaller in the fibrotic tissue. In addition, its mean values are in the ranges reported in [12] by using tagged MR. Therefore, it seems that our algorithm, using only cine images, has been able to recover averaged values of the strain of similar quality than those obtained using tagged MR. The lon-

gitudinal component of the strain has not been encountered significantly different in fibrotic and non-fibrotic tissue. Nevertheless, it should be stated that the computation of this component is rather complicated in these images because of the long spacing in the longitudinal direction (see Table 1) of SA images. Second, something similar occurs with the peak strain rate, where the absolute values of its radial and circumferential components have been encountered significantly smaller if fibrosis is present. Third, regarding the rotation angles, statistically significant differences have been encountered for the rotation in the LR plane, for which fibrotic regions present a smaller peak rotation dispersion than normal regions.

4. Conclusions

We have presented an image processing methodology for characterizing the mechanical behavior of fibrosis based on the fusion of LE and cine MR modalities and a novel material point tracking method. Using this methodology, statistically significant differences have been encountered between the mechanics of fibrotic and normal regions. Namely, fibrotic regions present a significantly smaller radial and circumferential deformation (as provided by the peak strain and strain rate). In addition, the rotation in the LR plane follows and anomalous pattern in fibrotic regions, as it presents a smaller variability than in normal regions. The major hypothesis to justify this behavior would be that the degree of contractility of fibrotic regions is further impaired with respect to the already impaired contractility [12] of normal zones. Nevertheless, these findings should be confirmed by incrementing the inferential power of the sample (p-values in Table 2 are just slightly below the 0.05 threshold) and by refining our processing methodology.

Acknowledgements

This work was supported in part by the MICIIN and the FEDER under grant TEC2010-17982, by the Instituto de Salud Carlos III under grant PI11-01492, and by the European Commission under grant FP7-223920.

References

[1] Karamitsos TD, Neubauer S. The interplay between cardiac strain and fibrosis in non-ischaemic cardiomyopathies: insights from cardiovascular magnetic resonance. Eur J Heart Fail 2011;13:927–928.

[2] Maron MS, Maron BJ, Harrigan C, Buros J, Gibson CM, Olivotto I, Biller L, Lesser JR, Udelson JE, Manning WJ, Appelbaum E. Hypertrophic cardiomyopathy phenotype revisited after 50 years with cardiovascular magnetic resonance. J Am Coll Cardiol 2009;54:220–228.

[3] Ismail TF, Hewins B, Jabbour A, Mistry N, Ferreira PF, Gulati A, Wage R, Clarysse P, Croisille P, Pennell DJ, Prasad SK. The relationship between interstitial fibrosis and contractile function in HCM: a combined T1-mapping and CSPAMM tagging study. J Cardiovasc Magn Reson 2012; 14:O97.

[4] Saito M, Okayama H, Yoshii T, Higashi H, Morioka H, Hiasa G, Sumimoto T, Inaba S, Nishimura K, Inoue K, Ogimoto A, Shigematsu Y, Hamada M, Higaki J. Clinical significance of global two-dimensional strain as a surrogate parameter of myocardial fibrosis and cardiac events in patients with hypertrophic cardiomyopathy. Eur Heart J Cardiovasc Imaging 2012;13:617–623.

[5] Chang SA, Lee SC, Choe YH, Hahn HJ, Jang SY, Park SJ, Choi JO, Park SW, Oh JK. Effects of hypertrophy and fibrosis on regional and global functional heterogeneity in hypertrophic cardiomyopathy. Int J Cardiovasc Imaging 2012; 28:133–140.

[6] Dass S, Suttie JJ, Piechnik SK, Ferreira VM, Holloway CJ, Banerjee R, Mahmod M, Cochlin L, Karamitsos TD, Robson MD, Watkins H, Neubauer S. Myocardial tissue characterization using magnetic resonance noncontrast T1 mapping in hypertrophic and dilated cardiomyopathy. Circ Cardiovasc Imaging 2012;5:726–733.

[7] Cordero-Grande L, Vegas-Sánchez-Ferrero G, Casaseca-de-la Higuera P, Alberola-López C. A Markov random field approach for topology-preserving registration: Application to object-based tomographic image interpolation. IEEE Trans Image Process 2012;21:2047–2061.

[8] Cordero-Grande L, Merino-Caviedes S, Albà X, Figueras i Ventura RM, Frangi AF, Alberola-López C. 3D fusion of cine and late-enhanced cardiac magnetic resonance images. In 9th IEEE ISBI. Barcelona (Spain), 2012; 286–289.

[9] Valette S, Chassery JM, Prost R. Generic remeshing of 3D triangular meshes with metric-dependent discrete Voronoi diagrams. IEEE Trans Vis Comput Graphics 2008;14:369–381.

[10] Si H, Gärtner K. Meshing piecewise linear complexes by constrained Delaunay tetrahedralizations. In Springer Int Mesh Round. 2005; 147–163.

[11] Cordero-Grande L, Martín-Fernández M, Alberola-López C. Integration of biomechanical properties in a Markov random field: Application to myocardial motion estimation in cardiomyopathy patients. In OSA QMI. Arlington, Virginia (USA), 2013; invited talk.

[12] Piella G, De Craene M, Bijnens BH, Tobon-Gómez C, Huguet M, Avegliano G, Frangi AF. Characterizing myocardial deformation in patients with left ventricular hypertrophy of different etiologies using the strain distribution obtained by magnetic resonance imaging. Rev Esp Cardiol 2010;63:1281–1291.

Address for correspondence:

Lucilio Cordero-Grande
Laboratorio de Procesado de Imagen, ETSIT, Universidad de Valladolid, Paseo de Belén 15, 47011, Valladolid, Spain
lcorgra@lpi.tel.uva.es